Spin polarized neutron matter within the Dirac-Brueckner-Hartree-Fock approach

F. Sammarruca
Physics Department, University of Idaho, Moscow, Idaho 83844, USA

P. G. Krastev
Physics Department, Texas A&M University-Commerce, Commerce, Texas 75429-3011, USA
(Received 11 September 2006; published 26 March 2007)

The relation between energy and density (known as the nuclear equation of state) plays a major role in a variety of nuclear and astrophysical systems. Spin and isospin asymmetries can have a dramatic impact on the equation of state and possibly alter its stability conditions. An example is the possible manifestation of ferromagnetic instabilities, which would indicate the existence, at a certain density, of a spin-polarized state with lower energy than the unpolarized one. This issue is being discussed extensively in the literature and the conclusions are presently very model dependent. We will report and discuss our recent progress in the study of spin-polarized neutron matter. The approach we take is microscopic and relativistic. The calculated neutron matter properties are derived from realistic nucleon-nucleon interactions. This makes it possible to understand the properties of the equation of state in terms of specific features of the nuclear force model.

DOI: 10.1103/PhysRevC.75.034315 PACS number(s): 21.65.+f, 21.30.Fe, 21.60.Jz, 26.60.+c

I. INTRODUCTION

The properties of dense and/or highly asymmetric nuclear matter, where *asymmetric* may refer to isospin or spin asymmetries, are of great current interest in nuclear physics and astrophysics. This topic is broad since it reaches out to exotic systems on the nuclear chart as well as, on a dramatically different scale, exotic objects in the universe such as compact stars.

In this paper, we investigate the bulk and single-particle properties of spin-polarized neutron matter. The study of the magnetic properties of dense matter is of considerable interest in conjunction with the physics of pulsars, which are believed to be rapidly rotating neutron stars with strong surface magnetic fields. The polarizability of nuclear matter can have strong effects on neutrino diffusion and, in turn, variations of the neutrino mean free path resulting from changes in the magnetic susceptibility of neutron matter can impact the physics of supernovae and proton-neutron stars.

The magnetic properties of neutron and nuclear matter have been studied extensively for a long time by many authors and with a variety of theoretical methods [1–29]. Nevertheless, conclusions about the possibility of a phase transition to a ferromagnetic state at some critical density are still contradictory. For instance, calculations based on Skyrme-type interactions [23] predict that such instabilities will occur with increasing density. In particular, currently used Skyrme forces show a ferromagnetic transition for neutron matter at densities between $1.1\rho_0$ and $3.5\rho_0$ [24]. However, more recent predictions based on Monte Carlo simulations [16] and the Brueckner-Hartree-Fock (BHF) approach with realistic nucleon-nucleon (*NN*) interactions [18,19] exclude these instabilities, at least at densities up to several times normal nuclear density. Similarly, no evidence of a transition to a ferromagnetic state was found in older calculations based on the BHF approach with the Reid hard-core potential as well as nonlocal separable potentials [10]. Relativistic calculations based on effective meson-nucleon Lagrangians [13] predict the ferromagnetic transition to take place at several times nuclear matter density, with its onset being crucially determined by the inclusion of the isovector mesons. Clearly, the existence of such a phase transition depends sensitively on the modeling of the spin-dependent part of the nuclear force and its behavior in the medium. Thus, this unsettled issue goes to the very core of nuclear physics.

Our calculation is microscopic and treats the nucleons relativistically. A parameter-free and internally consistent approach is important if we are to interpret our conclusions in terms of the underlying nuclear force. This is precisely our focus, namely to understand the in-medium behavior of specific components of the nuclear force (in this case, the spin dependence). Different *NN* potentials can have comparable quality, as seen from their global description of *NN* data, and yet differ in specific features. Thus, it will be interesting to explore how, for a given many-body approach, predictions for spin-polarized neutron matter depend upon specific features of the *NN* potential. Second, it will be insightful to compare with predictions based on a realistic *NN* potential and the BHF method [18], especially at the higher densities, where the repulsive Dirac effect can have a dramatic impact on the short-range nature of the force.

This work is organized in the following way: After the introductory notes in this section, we briefly review our theoretical framework (Sec. II); our results are presented and discussed in Sec. III; we conclude in Sec. IV with a short summary and outlook.

II. BRIEF DESCRIPTION OF THE CALCULATION

The starting point of any microscopic calculation of nuclear structure or reactions is a realistic free-space *NN* interaction. A realistic and quantitative model for the nuclear force with reasonable theoretical foundations is the one-boson-exchange

(OBE) model [30]. Unless otherwise specified, our standard framework consists of the Bonn B potential together with the Dirac-Brueckner-Hartree-Fock (DBHF) approach to nuclear matter. A detailed description of our application of the DBHF method to nuclear, neutron, and asymmetric matter can be found in our earlier works [31–33].

Similarly to what we have done to describe isospin asymmetries of nuclear matter, we write the single-particle potential as the solution of a set of coupled equations,

$$U_u = U_{ud} + U_{uu}, \tag{1}$$

$$U_d = U_{du} + U_{dd}, \tag{2}$$

where u and d refer to "up" and "down" polarizations, respectively, and where each $U_{\sigma\sigma'}$ term contains the appropriate (spin-dependent) part of the interaction, $G_{\sigma\sigma'}$. More specifically,

$$U_\sigma(\vec{p}) = \sum_{\sigma'=u,d} \sum_{q \leqslant k_F^{\sigma'}} \langle \sigma, \sigma' | G(\vec{p}, \vec{q}) | \sigma, \sigma' \rangle, \tag{3}$$

where the second summation indicates integration over the two Fermi seas of spin-up and spin-down neutrons, and

$$\begin{aligned} &\langle \sigma, \sigma' | G(\vec{p}, \vec{q}) | \sigma, \sigma' \rangle \\ &= \sum_{L,L',S,J,M,M_L} \left\langle \frac{1}{2}\sigma; \frac{1}{2}\sigma' \middle| S(\sigma+\sigma') \right\rangle \left\langle \frac{1}{2}\sigma; \frac{1}{2}\sigma' \middle| S(\sigma+\sigma') \right\rangle \langle L M_L; S(\sigma+\sigma') | J M \rangle \\ &\quad \times \langle L' M_L; S(\sigma+\sigma') | J M \rangle i^{L'-L} Y^*_{L',M_L}(\hat{k}_{\rm rel}) \\ &\quad \times Y_{L,M_L}(\hat{k}_{\rm rel}) \langle L S J | G(k_{\rm rel}, K_{\rm c.m.}) | L' S J \rangle. \end{aligned} \tag{4}$$

The notation $\langle j_1 m_1; j_2 m_2 | j_3 m_3 \rangle$ is used for the Clebsh-Gordon coefficients. Clearly, the need to separate the interaction by individual spin components brings along angular dependence, with the result that the single-particle potential depends also on the direction of the momentum. Notice that the G-matrix equation is solved by using partial wave decomposition and the matrix elements are then summed as in Eq. (4) to provide the new matrix elements in the uncoupled-spin representation needed for Eq. (3). The three-dimensional integration in Eq. (3) is performed in terms of the spherical coordinates of $\vec{q}$, (q, θ_q, ϕ_q), with the final result depending upon both magnitude and direction of $\vec{p}$. However, the scattering equation is solved by using relative and center-of-mass coordinates, $k_{\rm rel}$ and $K_{\rm c.m.}$. These are easily related to the momenta of the two particles in the nuclear matter rest frame through the standard definitions $\vec{K}_{\rm c.m.} = \vec{p} + \vec{q}$ and $\vec{k}_{\rm rel} = \frac{\vec{p}-\vec{q}}{2}$. (The latter displays the dependence of the argument of the spherical harmonics upon $\vec{p}$ and $\vec{q}$.)

Solving the G-matrix equation requires knowledge of the single-particle potential, which in turn requires knowledge of the interaction. Hence, Eqs. (1) and (2) together with the G-matrix equation constitute a self-consistency problem, which is handled, technically, exactly the same way as previously done for the case of isospin asymmetry [31]. The Pauli operator for scattering of two particles with unequal Fermi momenta, contained in the kernel of the G-matrix equation, is also defined in perfect analogy with the isospin-asymmetric one [31],

$$Q_{\sigma\sigma'}(p, q, k_F^\sigma, k_F^{\sigma'}) = \begin{cases} 1 & \text{if} \quad p > k_F^\sigma \ \text{ and } \ q > k_F^{\sigma'}, \\ 0 & \text{otherwise.} \end{cases} \tag{5}$$

Notice that, although a full three-dimensional integration is performed in Eq. (3), the usual angle-average procedure is applied to the Pauli operator (when expressed in terms of $k_{\rm rel}$ and $K_{\rm c.m.}$) and to the two-particle propagator in the kernel of the G-matrix equation.

Once a self-consistent solution is obtained for the single-particle spectrum, the average potential energy for particles with spin polarization σ is obtained as

$$\langle U_\sigma \rangle = \frac{1}{2} \frac{1}{(2\pi)^3} \frac{1}{\rho_\sigma} \int_{p=0}^{k_F^\sigma} \int_{\theta_p=0}^{\pi} \int_{\phi_p=0}^{2\pi} U_\sigma(\vec{p}) p^2 dp d\Omega_p. \tag{6}$$

The average potential energy per particle is then

$$\langle U \rangle = \frac{\rho_u \langle U_u \rangle + \rho_d \langle U_d \rangle}{\rho}. \tag{7}$$

The kinetic energy (or, rather, the free-particle operator in the Dirac equation within the DBHF framework) is also averaged over magnitude and direction of the momentum. In particular, we calculate the average free-particle energy for spin-up(down) neutrons as

$$\langle T_\sigma \rangle = \frac{\int d\Omega \bar{T}(m^*_\sigma(\theta))}{\int d\Omega}, \tag{8}$$

where $\bar{T}$ is the average over the magnitude of the momentum. Notice that the angular dependence comes in through the effective masses, which, being part of the parametrization of the single-particle potential, are themselves direction dependent (and of course different for spin-up or spin-down neutrons).

Finally,

$$\langle T \rangle = \frac{\rho_u \langle T_u \rangle + \rho_d \langle T_d \rangle}{\rho} \tag{9}$$

and the average energy per neutron is

$$\bar{e} = \langle U \rangle + \langle T \rangle. \tag{10}$$

As in the case of isospin asymmetry, it can be expected that the dependence of the average energy per particle upon the degree of polarization [18] will follow the law

$$\bar{e}(\rho, \beta) = \bar{e}(\rho, \beta = 0) + S(\rho)\beta^2, \tag{11}$$

where β is the spin asymmetry, defined by $\beta = \frac{\rho_u - \rho_d}{\rho}$. A negative value of $S(\rho)$ would signify that a polarized system is more stable than unpolarized neutron matter.

From the energy shift,

$$S(\rho) = \bar{e}(\rho, \beta = 1) - \bar{e}(\rho, \beta = 0), \tag{12}$$

the magnetic susceptibility can be easily calculated. If the parabolic dependence is assumed, then one can write the

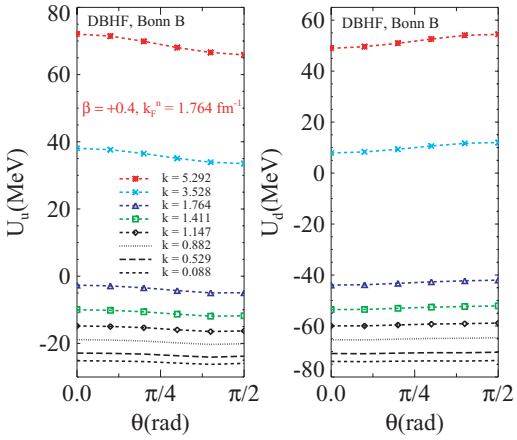

FIG. 1. (Color online) Angular dependence of the single-particle potential for spin-up and spin-down neutrons at fixed spin asymmetry and Fermi momentum and for different values of the neutron momentum. The momenta are in units of fm^{-1}. The angle is defined relative to the polarization axis.

magnetic susceptibility as [18]

$$\chi = \frac{\mu^2 \rho}{2S(\rho)}, \tag{13}$$

where μ is the neutron magnetic moment. The magnetic susceptibility in often expressed in units of χ_F, the magnetic susceptibility of a free Fermi gas,

$$\chi_F = \frac{\mu^2 m}{\hbar^2 \pi^2} k_F, \tag{14}$$

where k_F denotes the average Fermi momentum, which is related to the total density by

$$k_F = (3\pi^2 \rho)^{1/3}. \tag{15}$$

The Fermi momenta for up and down neutrons are

$$\begin{aligned} k_F^u &= k_F(1+\beta)^{1/3}, \\ k_F^d &= k_F(1-\beta)^{1/3}. \end{aligned} \tag{16}$$

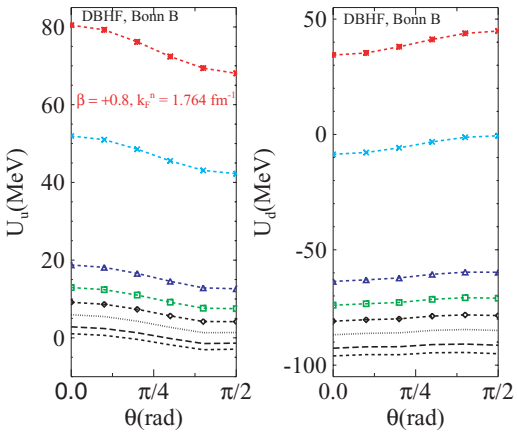

FIG. 2. (Color online) Same as Fig. 1 but for a larger value of the spin asymmetry.

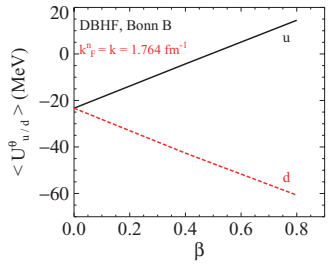

FIG. 3. (Color online) Asymmetry dependence of the single-particle potential for spin-up and spin-down neutrons at fixed density and momentum. The angular dependence is integrated out.

For the most general case, it will be necessary to combine isospin and spin asymmetry. With twice as many degrees of freedom, the coupled self-consistency problem schematically displayed in Eqs. (1) and (2) is numerically more involved but straightforward. This is left to a future work.

III. RESULTS AND DISCUSSION

We begin by showing the angular and momentum dependence of the single-neutron potential (see Figs. 1 and 2). The angular dependence is rather mild, especially at the lowest momenta. As can be reasonably expected, it becomes stronger at larger values of the asymmetry (see Fig. 2). In Fig. 3, the asymmetry dependence is displayed for fixed density and momentum (with the angular dependence averaged out). As the density of u particles goes up, with the total density remaining constant, the most likely kind of interaction for u neutrons is of the uu type. Similarly, the largest contribution to the d-particle potential is of the du type [see Eqs. (1) and (2)], with the latter being apparently more attractive, as can be inferred by the spin splitting of the potential shown in Fig. 3. Before we move on to discuss this issue in greater detail, we also show the effective masses of u and d neutrons (see Fig. 4) and observe that they display a qualitatively similar behavior to that of the corresponding single-particle potentials. The average energy per particle at various densities and as a function of the asymmetry parameter is shown in the third frame of Fig. 5. The first two frames display the contribution from the average potential energy and the average kinetic energy, respectively. The parabolic dependence on β (i.e., linear on β^2) is obviously verified. In Fig. 6 we show

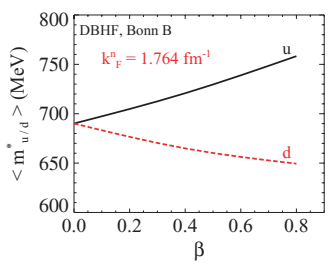

FIG. 4. (Color online) Asymmetry dependence of the effective masses for upward and downward polarized neutrons under the same conditions as in Fig. 3.

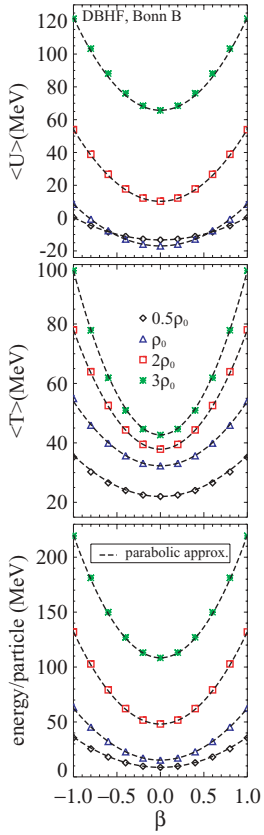

FIG. 5. (Color online) Average potential, kinetic, and total energy per particle at various densities as a function of the spin asymmetry. Predictions have been obtained with our standard DBHF calculation.

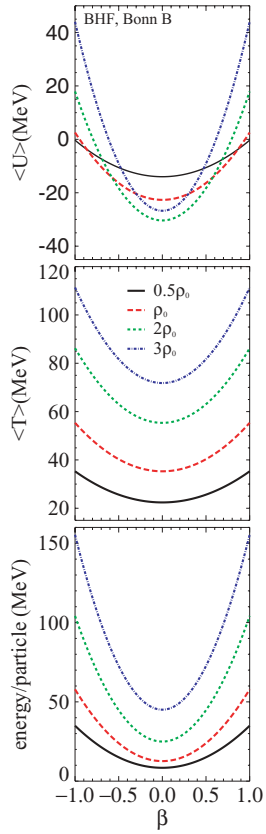

FIG. 6. (Color online) Same as Fig. 5 but for predictions obtained with the BHF calculation.

the corresponding predictions obtained with the conventional BHF approach. This comparison may be quite insightful, as we further discuss next. We notice that the Dirac energies are overall more repulsive, but the parabolas predicted with the BHF prescription appear to become steeper, relative to each other, as density grows. The energy difference between the totally polarized state and the unpolarized one for both the relativistic and the nonrelativistic calculation is shown in Fig. 7. Although the DBHF curve is initially higher, its growth shows a tendency to slow down and the two sets of predictions cross over just above $3\rho_0$.

Before leaving this detour into the nonrelativistic model, we observe that the predictions shown in Fig. 6 are reasonably consistent with those from previous studies that used the BHF approach and the Nijmegen II and Reid93 *NN* potentials [18]. In fact, comparison with that work allows us to make some useful observations concerning the choice of a particular *NN* potential, for a similar many-body approach (in this case, BHF). We must keep in mind that off-shell differences exist among *NN* potentials (even if they are nearly equivalent in their fit of *NN* scattering data) and those will impact the *G* matrix (which, unlike the *T* matrix, is not constrained by the two-body data). Furthermore, off-shell differences will have a larger impact at high Fermi momenta, where the higher momentum components of the *NN* potential (usually also the most model dependent ones) play a larger role in the calculation. Accordingly, the best agreement between our

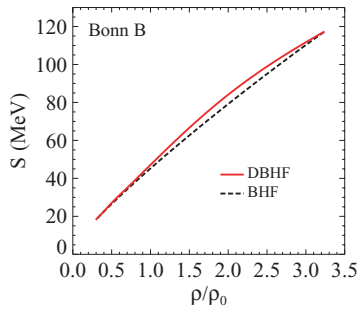

FIG. 7. (Color online) Energy difference between the polarized and the unpolarized states corresponding to Figs. 5 and 6.

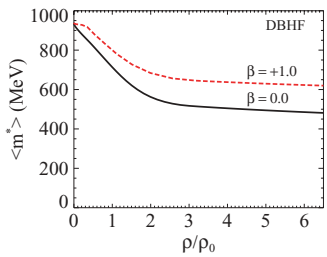

FIG. 8. (Color online) Neutron effective masses used in the DBHF calculations of the equation of state. The angular dependence is averaged out.

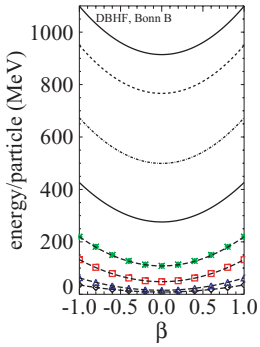

FIG. 9. (Color online) Average energy per particle at densities equal to 0.5, 1, 2, 3, 5, 7, 9, and 10 times ρ_0 (from lowest to highest curve). Predictions have been obtained with our DBHF calculation.

BHF predictions and those of Ref. [18] is seen at low to moderate densities. Furthermore, as far as differences based on the choice of the *NN* potential are concerned, we would expect them to be more pronounced for nuclear matter than for pure neutron matter, since the largest variations among modern realistic potentials are typically found in the strength of the tensor force, which is stronger in $T = 0$ partial waves (obviously absent in the *nn* system). This point will be explored in a later investigation.

In the remainder of this paper, we will focus on the DBHF model, which is our standard operational approach. To further explore the possibility of a ferromagnetic transition, we have extended the DBHF calculation to densities as high as $10\rho_0$.

The same method as described in Ref. [33] is applied to obtain the energy per particle where a self-consistent solution cannot be obtained (see Sec. III of Ref. [33] for details). The (angle-averaged) neutron effective masses for both the unpolarized and the fully polarized case are shown in Fig. 8 as a function of density. DBHF predictions for the average energy per particle are shown in Fig. 9 at densities ranging from $\rho = 0.5\rho_0$ to $10\rho_0$. What we observe is best seen through the spin-symmetry energy, which we calculate from Eq. (12) and show in Fig. 10. We see that at high density the energy shift between polarized and unpolarized matter continues to grow, but at a smaller rate, and eventually appears to saturate. Similar observations already made in conjunction with isospin asymmetry were explained in terms of stronger short-range repulsion in the Dirac model [33]. It must be

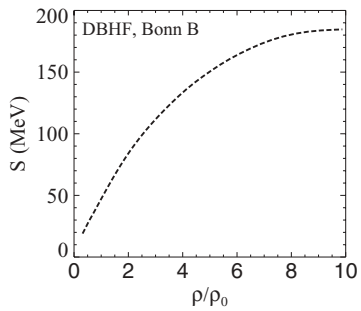

FIG. 10. Density dependence of the spin symmetry energy obtained with the DBHF model.

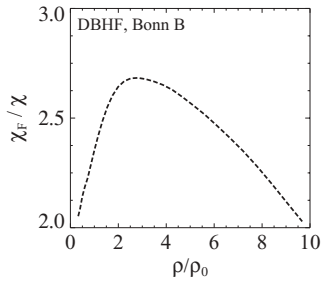

FIG. 11. Density dependence of the ratio χ_F/χ. Predictions are obtained with the DBHF model.

kept in mind that some large contributions, such as the one from the $^1S_0$ state, are not allowed in the fully polarized case. Now, if such contributions (which are typically attractive at normal densities) become more and more repulsive with density (owing to the increasing importance of short-range repulsive effects), their absence will amount to less repulsive energies at high density. In contrast, if large and attractive singlet partial waves remain attractive up to high densities, their suppression (which is demanded in the totally polarized case) will effectively amount to increased repulsion.

In conclusion, although the curvature of the spin-symmetry energy may suggest that ferromagnetic instabilities are in principle possible within the Dirac model, inspection of Fig. 10 reveals that such a transition does not take place at least up to $10\rho_0$. Clearly, it would not be appropriate to explore even higher densities without additional considerations, such as transition to a quark phase. In fact, even on the high side of the densities considered here, softening of the equation of state from additional degrees of freedom not included in the present model may be necessary to draw a more definite conclusion.

Finally, in Fig. 11 we show the ratio χ_F/χ, whose behavior is directly related to the spin-symmetry energy [see Eq. (13)]. Clearly, similar observations apply to both Fig. 11 and Fig. 10. [The magnetic susceptibility would show an infinite discontinuity, corresponding to a sign change of $S(\rho)$, in case of a ferromagnetic instability.]

IV. CONCLUSIONS

We have calculated bulk and single-particle properties of spin-polarized neutron matter. The equations of state we obtain with the DBHF model are generally rather repulsive at the larger densities. The energy of the unpolarized system (where all *nn* partial waves are allowed) grows rapidly at high density with the result that the energy difference between totally polarized and unpolarized neutron matter tends to slow down with density. This may be interpreted as a *precursor* of spin-separation instabilities, although no such transition is actually seen up to $10\rho_0$. Our analysis allowed us to locate the origin of this behavior in the contributions to the energy from specific partial waves and their behavior in the medium, particularly increased repulsion in the singlet states.

In future work, the impact of further extensions will be considered. These include examining the effects of contributions

that soften the equation of state (especially at high density), extending our framework to incorporate both spin- and isospin-asymmetries, and examining the temperature dependence of our observations for spin- and isospin-asymmetries of neutron and nuclear matter.

ACKNOWLEDGEMENT

The authors acknowledge financial support from the U.S. Department of Energy under Grant No. DE-FG02-03ER41270.

[1] D. H. Brownell and J. Callaway, Nuovo Cimento B **60**, 169 (1969).
[2] M. J. Rice, Phys. Lett. **A29**, 637 (1969).
[3] J. W. Clark and N. C. Chao, Lettere Nuovo Cimento **2**, 185 (1969).
[4] J. W. Clark, Phys. Rev. Lett. **23**, 1463 (1969).
[5] S. D. Silverstein, Phys. Rev. Lett. **23**, 139 (1969).
[6] E. Østgaard, Nucl. Phys. **A154**, 202 (1970).
[7] J. M. Pearson and G. Saunier, Phys. Rev. Lett. **24**, 325 (1970).
[8] V. R. Pandharipande, V. K. Garde, and J. K. Srivastava, Phys. Lett. **B38**, 485 (1972).
[9] S.-O. Bäckmann, C.-G. Källman, and O. Sjöberg, Phys. Lett. **B43**, 263 (1973).
[10] P. Haensel, Phys. Rev. C **11**, 1822 (1975).
[11] A. D. Jackson, E. Krotscheck, D. E. Meltzer, and R. Smith, Nucl. Phys. **A386**, 125 (1982).
[12] J. Dabrowski, Can. J. Phys. **62**, 400 (1984).
[13] S. Marcos, R. Niembro, M. L. Quelle, and J. Navarro, Phys. Lett. **B271**, 277 (1991).
[14] M. Kutshera and W. Wojcik, Phys. Lett. **B223**, 11 (1989).
[15] P. Bernardos, S. Marcos, R. Niembro, and M. L. Quelle, Phys. Lett. **B356**, 175 (1995).
[16] S. Fantoni, A. Sarsa, and K. E. Schmidt, Phys. Rev. Lett. **87**, 181101 (2001).
[17] T. Frick, H. Müther, and A. Sedrakian, Phys. Rev. C **65**, 061303(R) (2002).
[18] I. Vidaña, A. Polls, and A. Ramos, Phys. Rev. C **65**, 035804 (2002).
[19] I. Vidaña and I. Bombaci, Phys. Rev. C **66**, 045801 (2002).
[20] A. A. Isayev and J. Yang, Phys. Rev. C **69**, 025801 (2004).
[21] F. L. Braghin, Phys. Rev. C **71**, 064303 (2005).
[22] N. Kaiser, Phys. Rev. C **70**, 054001 (2004).
[23] A. Rios, A. Polls, and I. Vidaña, Phys. Rev. C **71**, 055802 (2005).
[24] M. Kutshera and W. Wojcik, Phys. Lett. **B325**, 271 (1994).
[25] A. Vidaurre, J. Navarro, and J. Bernabéu, Astron. Astrophys. **135**, 361 (1984).
[26] I. Bombaci, A. Polls, A. Ramos, A. Rios, and I. Vidaña, Phys. Lett. **B632**, 638 (2006).
[27] V. S. Uma Maheswari, D. N. Basu, J. N. De, and S. K. Samaddar, Nucl. Phys. **A615**, 516 (1997).
[28] W. Zuo, U. Lombardo, and C. W. Shen, in *Quark-Gluon Plasma and Heavy Ion Collisions*, edited by W. M. Alberico *et al*. (World Scientific, Singapore, 2002), p. 192.
[29] W. Zuo, C. Shen, and U. Lombardo, Phys. Rev. C **67**, 037301 (2003).
[30] R. Machleidt, Adv. Nucl. Phys. **19**, 189 (1989).
[31] D. Alonso and F. Sammarruca, Phys. Rev. C **67**, 054301 (2003).
[32] F. Sammarruca, W. Barredo, and P. Krastev, Phys. Rev. C **71**, 064306 (2005).
[33] P. G. Krastev and F. Sammarruca, Phys. Rev. C **74**, 025808 (2006).